

Supporting Information:

Orbital Forcing of the Paleocene and Eocene Carbon Cycle

Richard E. Zeebe^{1,*}, Thomas Westerhold², Kate Littler³, and James C. Zachos⁴

*Corresponding Author.

¹School of Ocean and Earth Science and Technology, University of Hawaii at Manoa, 1000 Pope Road, MSB 629, Honolulu, HI 96822, USA. zeebe@soest.hawaii.edu

²MARUM, University of Bremen, D-28359 Bremen, Germany. twesterhold@marum.de

³Camborne School of Mines, University of Exeter, Penryn, Cornwall TR10 9FE, UK. K.Littler@exeter.ac.uk

⁴Earth and Planetary Sciences Department, University of California, Santa Cruz, USA. jzachos@ucsc.edu

February 28, 2017

Paleoceanography

S1 Supporting Figures

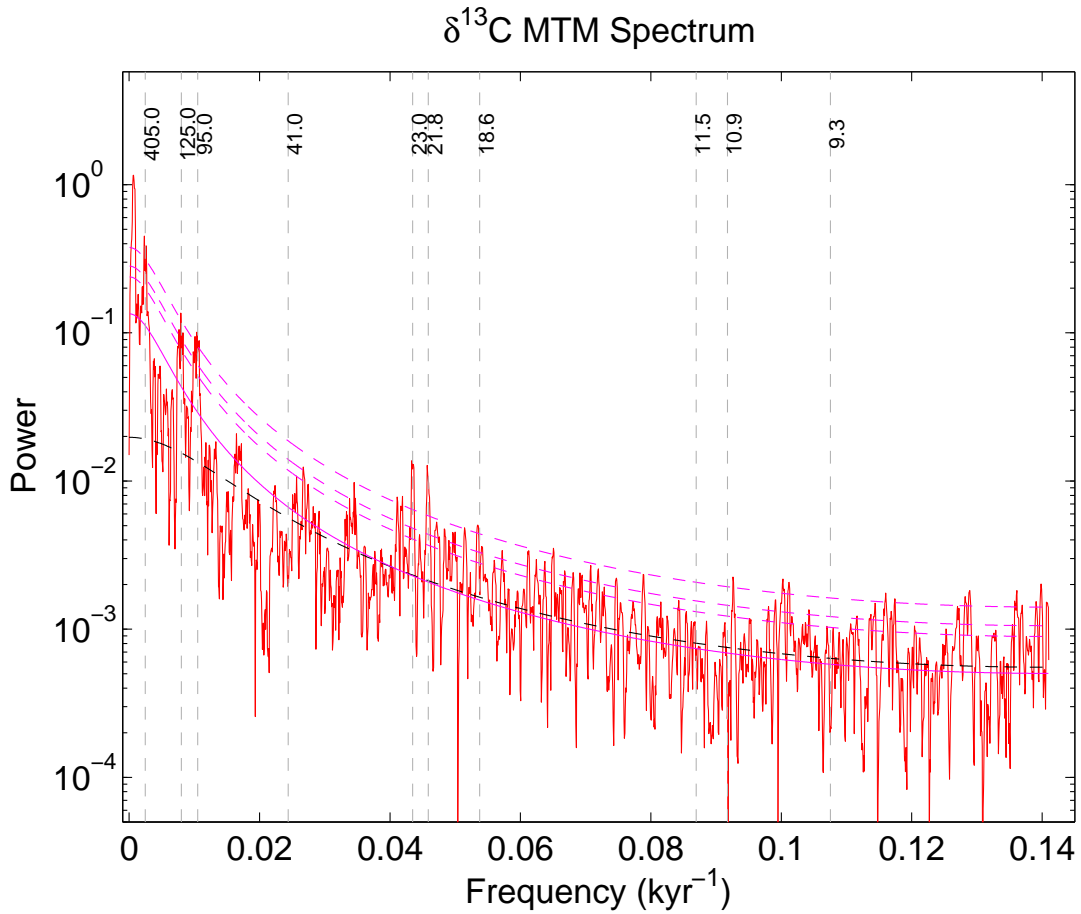


Figure S1. MTM spectrum up to Nyquist frequency ($f_N = 0.14 \text{ kyr}^{-1}$) of the benthic carbon isotope record from ODP Site 1262 [Little et al., 2014] (cf. main paper, Fig. 1). Note lack of large peaks in the half-precession band at 11.5 and 9.3 kyr compared to precession peaks at 23 and 18.6 kyr. Other peak heights in the half-precession band are similar to various (random?) peaks at $f \gtrsim 0.11 \text{ kyr}$.

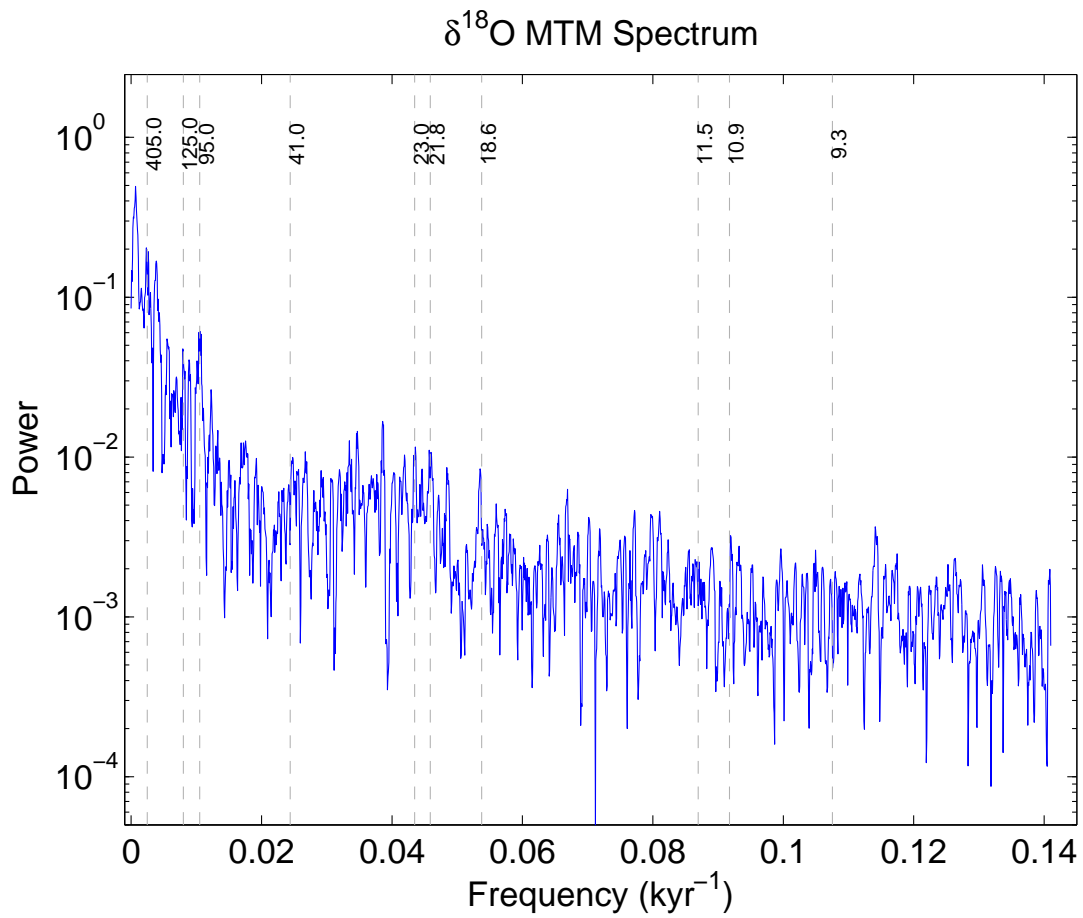


Figure S2. MTM spectrum up to Nyquist frequency ($f_N = 0.14 \text{ kyr}^{-1}$) of the benthic oxygen isotope record from ODP Site 1262 [Little *et al.*, 2014].

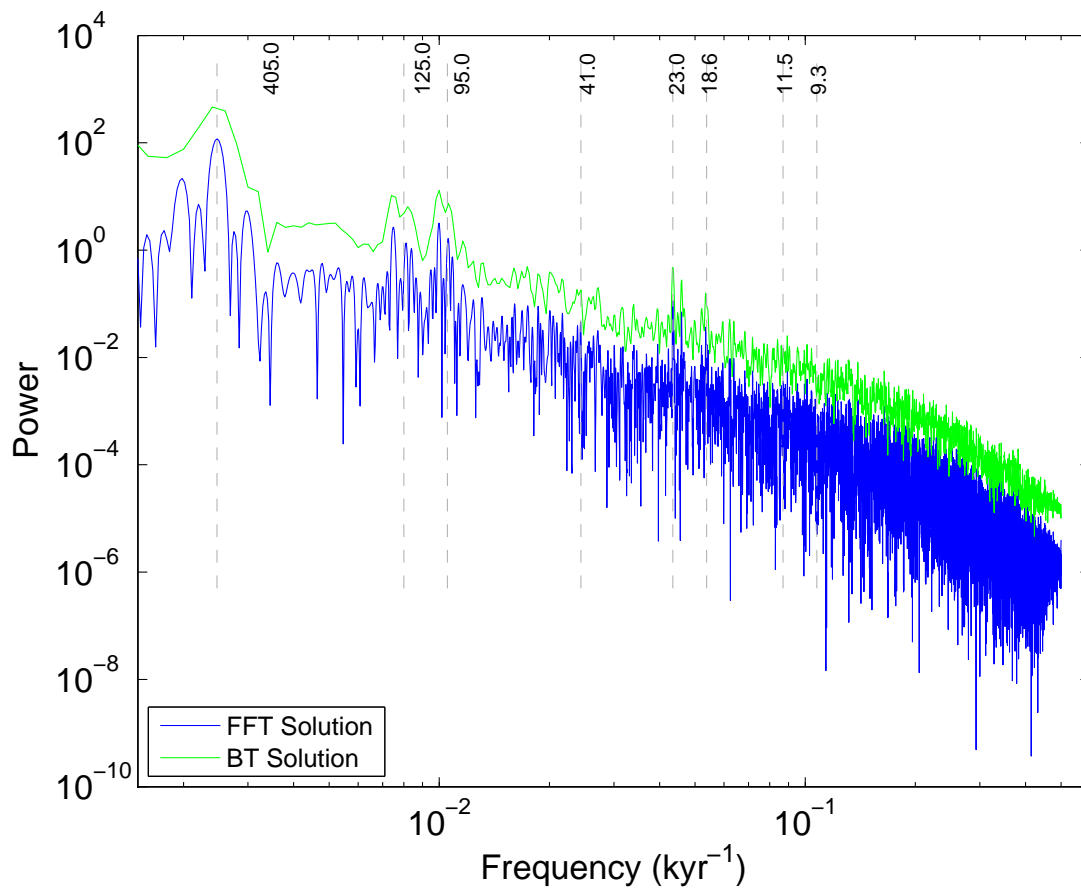


Figure S3. Power spectrum of the minimal carbon cycle model up to Nyquist frequency, f_N (cf. main paper, Fig. 4). The numerical solution was resampled at 1 kyr (hence $f_N = 0.5 \text{ kyr}^{-1}$) and zero-padded. Note logarithmic frequency axis.

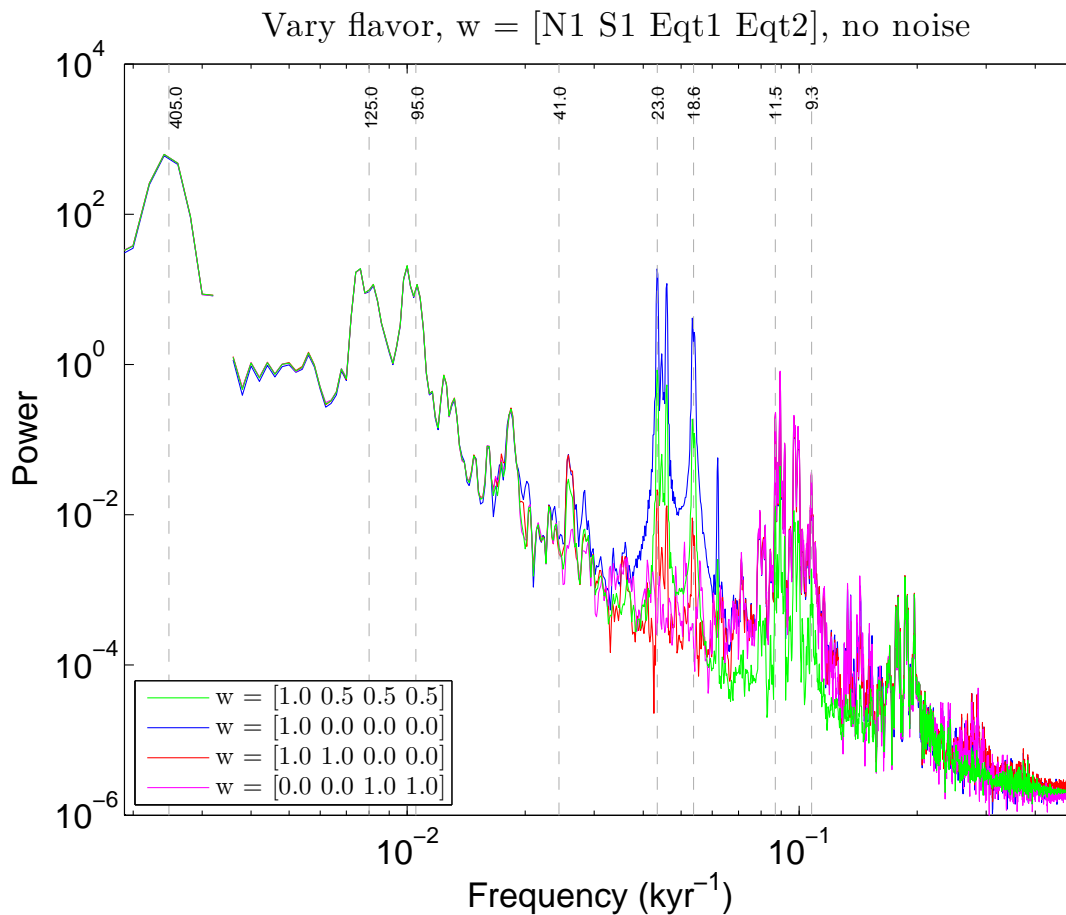


Figure S4. Blackman-Tukey spectrum (1/2 lags) of the minimal carbon cycle model up to Nyquist frequency (f_N) for different forcing flavors, without noise (cf. main paper, Fig. 5). The numerical solution was resampled at 1 kyr (hence $f_N = 0.5 \text{ kyr}^{-1}$). Note logarithmic frequency axis. Due to clipped/DC'd forcing, all flavors produce some power in the half-precession band, which is, however, masked to varying degrees when noise is included (main paper, Fig. 5).

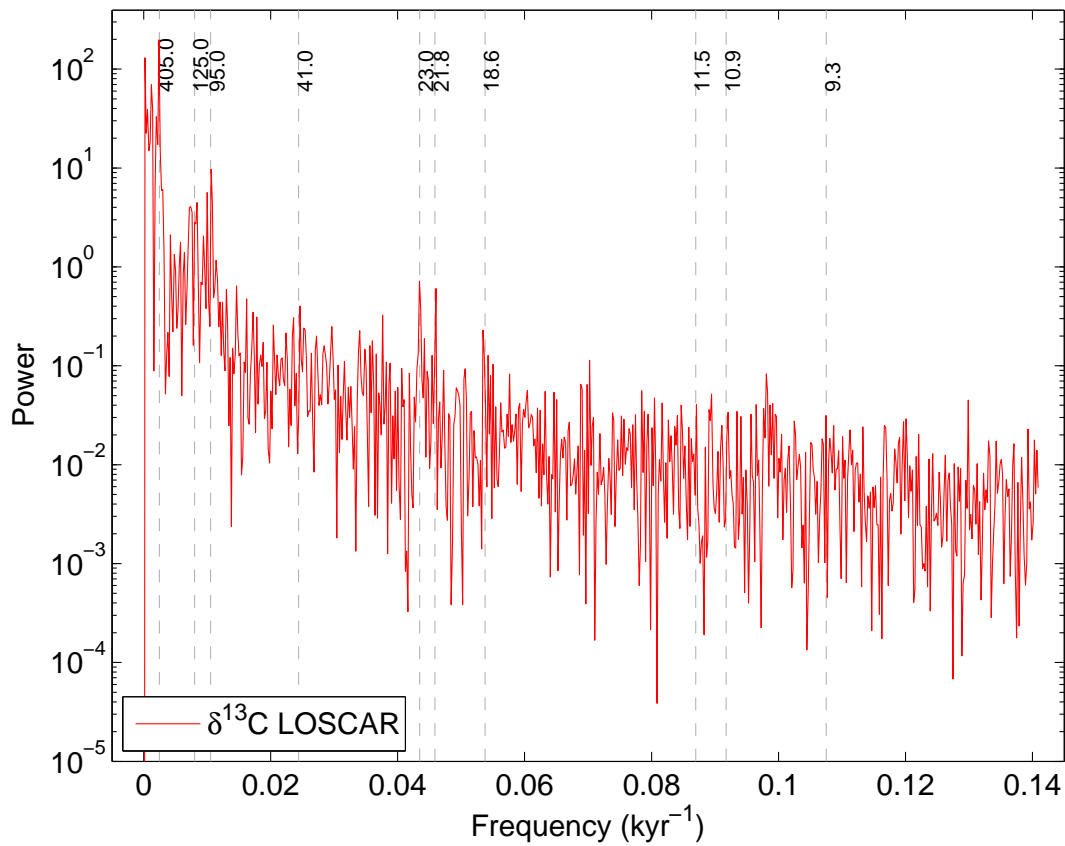


Figure S5. LOSCAR's $\delta^{13}\text{C}$ power spectrum up to Nyquist frequency, f_N (cf. main paper, Fig. 9). The numerical solution was resampled at the 1262-benthic isotope resolution of ~ 3.5 kyr (hence $f_N = 0.14 \text{ kyr}^{-1}$).

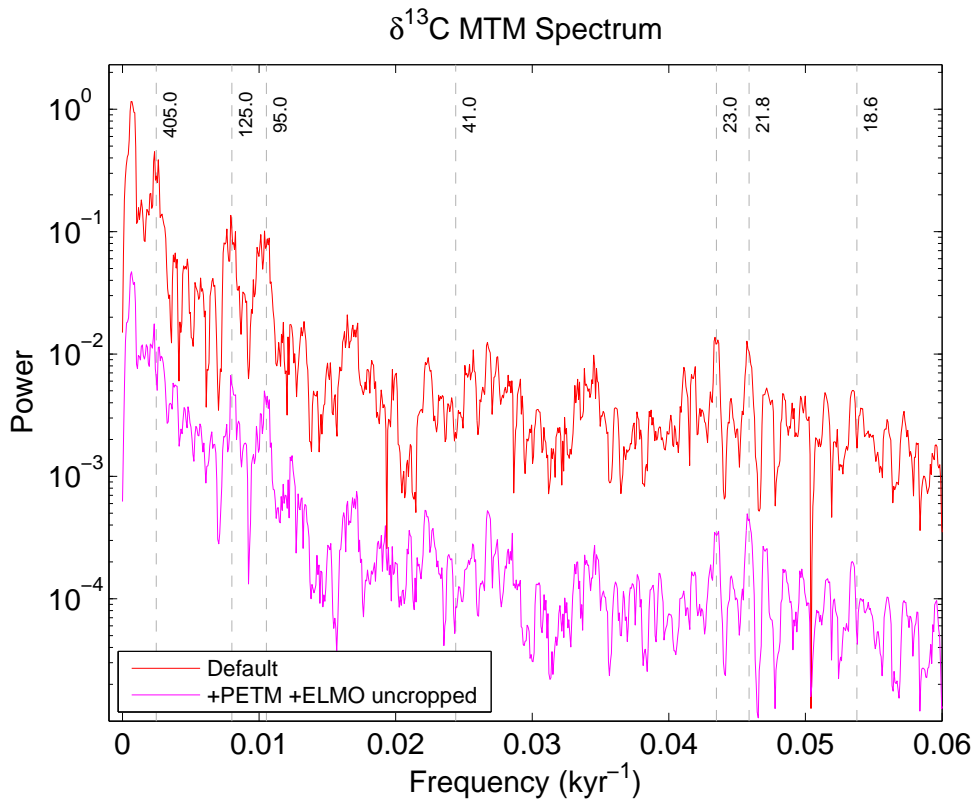


Figure S6. MTM spectrum of the benthic carbon isotope record from ODP Site 1262 [Littler *et al.*, 2014] (red = default as in main paper, Fig. 1) and including PETM and ELMO, uncropped (magenta). The spectra are very similar, except for the 405-kyr peak, which is weakened when including the hyperthermals. This is almost entirely due to the large CIE at the PETM (ELMO makes little difference). As the PETM onset appears to be out-of-phase with the 405-kyr cycle [Cramer *et al.*, 2003; Zachos *et al.*, 2010; Littler *et al.*, 2014], the large PETM-CIE disrupts the 405-kyr cycle, leading to a weakened 405-kyr peak in the spectrum.

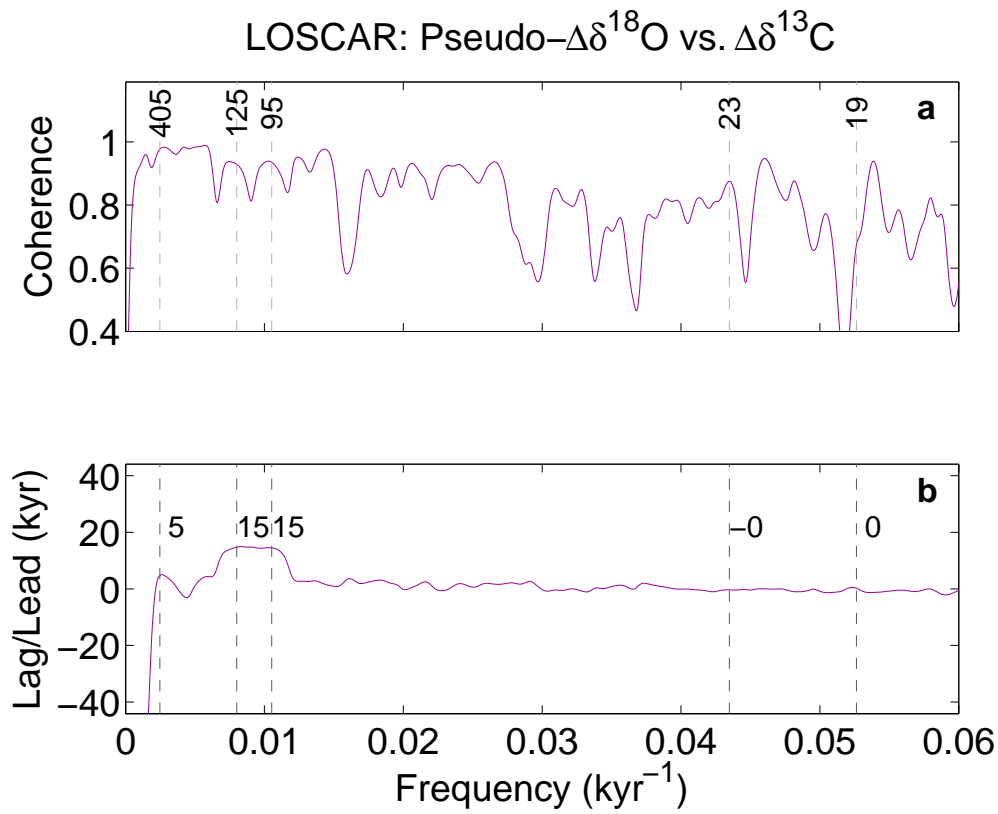


Figure S7. Coherence and phase lag of $\Delta\delta^{18}\text{O}$ vs. $\Delta\delta^{13}\text{C}$ of insolation + noise forced LOSCAR runs for C_{org} burial + global solar temperature. Coherence and phase (leads/lags) were computed using MATLAB's cross power spectral density estimates based on Welch's method (pwelch.m, cpsd.m) with 8 windows and 50% overlap. (a) Coherence. Vertical dashed lines indicate periods (\mathcal{T} , kyr). (b) Phase. Numbers (kyr) next to dashed lines indicate leads/lags at \mathcal{T} , positive for $\Delta\delta^{18}\text{O}$ lead.

S2 $\Delta\delta^{18}\text{O}-\Delta\delta^{13}\text{C}$ slope vs. long-term $\delta^{18}\text{O}-\delta^{13}\text{C}$ trends

The $\Delta\delta^{18}\text{O}-\Delta\delta^{13}\text{C}$ slope per bin (S_{Δ}) provides information both on the covariance and the long-term (mostly secular) trends of $\delta^{18}\text{O}-\delta^{13}\text{C}$ (\dot{S}) across the considered time window (see main paper). On short time intervals, the covariance tends to dominate, on long intervals, the secular trends tend to dominate. For example, for the 15 bins of the detrended records covering ~ 0.5 myr each (see main paper), S_{Δ} mostly reflects the relative amplitude of variations on sub-orbital and orbital time scale up to the 405-kyr cycle because such variations are usually larger than \dot{S} over 0.5 myr. The detrended and binned records (0.5 myr windows) are hence relevant to the discussion of forcing and response of carbon cycle and climate on orbital time scale (see main paper).

If instead, S_{Δ} is calculated without detrending, the result reflects more of a blend between covariance and long-term trends, depending on window size. This is best illustrated by using larger time windows, i.e., a smaller number of bins (say, 5 bins covering ~ 1.5 myr each, Fig. S8). For the bins at the edges around 54 and 60 Ma, the secular trends in $\delta^{13}\text{C}$ and $\delta^{18}\text{O}$ are similar and moderate in size (Fig. S8b). Hence S_{Δ} mostly reflects the covariance, which is (relatively) larger in $\delta^{18}\text{O}$ compared to $\delta^{13}\text{C}$ around 54 than around 60 Ma. Around 59 Ma, the $\delta^{13}\text{C}$ -trend is reversed up to the PCIM, hence the negative sign of S_{Δ} . Between 57 and 55 Ma, the $\delta^{18}\text{O}$ -variance is larger than around 60 Ma but is partly compensated for by the (relatively) larger negative secular trend in $\delta^{13}\text{C}$ (Fig. S8b). The long-term trends are pertinent to secular changes in carbon cycling and climate on multi-million year time scale [e.g. Komar *et al.*, 2013], rather than rhythmic carbon release and burial on orbital time scale.

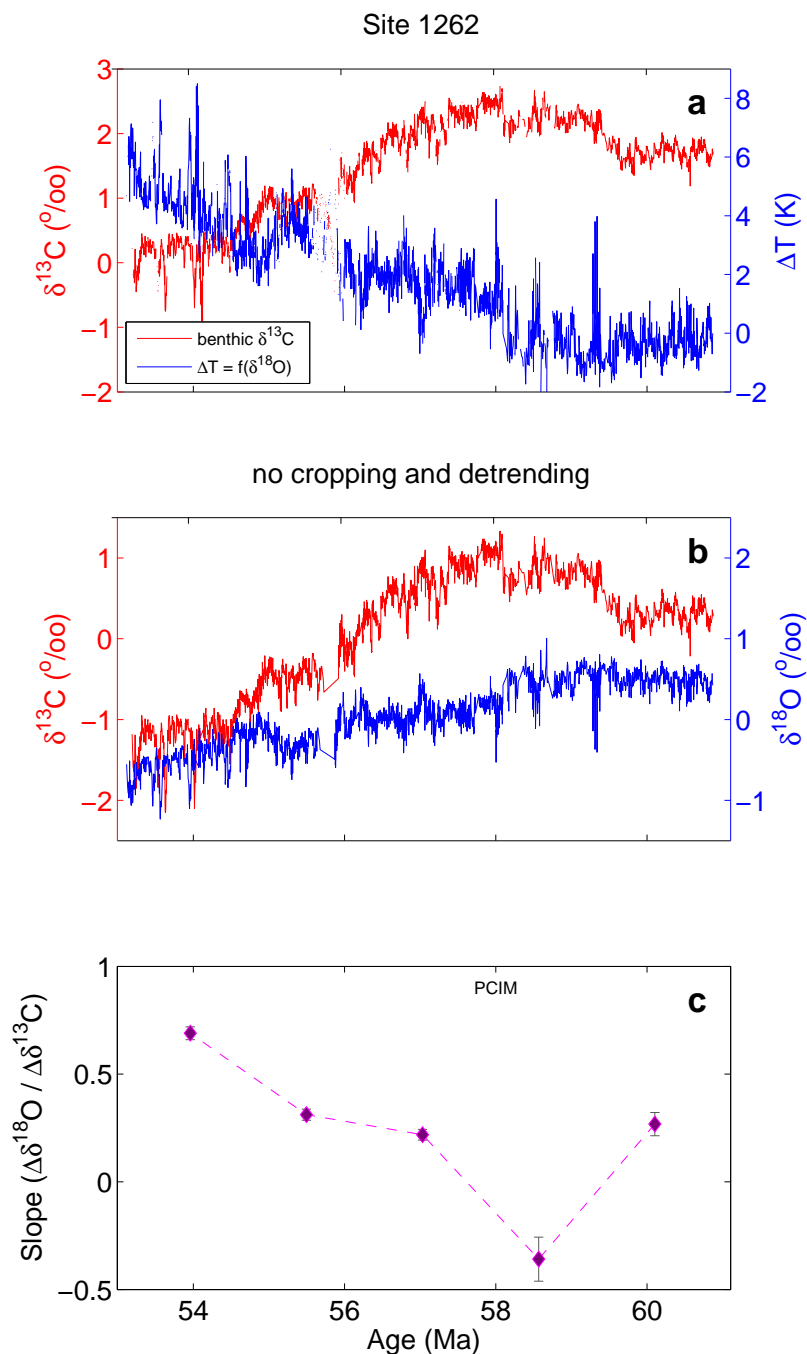


Figure S8. Long-term warming trend and $\Delta\delta^{18}\text{O}-\Delta\delta^{13}\text{C}$ slope over time. (a) Benthic $\delta^{13}\text{C}$ and $\delta^{18}\text{O}$ from Site 1262 ($\delta^{18}\text{O}$ converted to ice-free temperature change). (b) Time series without cropping and detrending. (c) Slopes for 5 bins of the data in (b), covering ~ 1.5 myr each (20% overlap). Error bars are based on regression for each bin.

References

- Cramer, B. S., J. D. Wright, D. V. Kent, and M.-P. Aubry, Orbital climate forcing of $\delta^{13}\text{C}$ excursions in the late Paleocene-early Eocene (chrons C24n-C25n), *Paleoceanogr.*, *18*, 1097, doi:10.1029/2003PA000909, 2003.
- Komar, N., R. E. Zeebe, and G. R. Dickens, Understanding long-term carbon cycle trends: The late Paleocene through the early Eocene, *Paleoceanogr.*, *28*, 650–662, doi:10.1002/palo.20060, 2013.
- Littler, K., U. Röhl, T. Westerhold, and J. C. Zachos, A high-resolution benthic stable-isotope record for the South Atlantic: Implications for orbital-scale changes in Late Paleocene-Early Eocene climate and carbon cycling, *Earth Planet. Sci. Lett.*, *401*, 18–30, doi:10.1016/j.epsl.2014.05.054, 2014.
- Zachos, J. C., H. McCarren, B. Murphy, U. Röhl, and T. Westerhold, Tempo and scale of late Paleocene and early Eocene carbon isotope cycles: Implications for the origin of hyperthermals, *Earth Planet. Sci. Lett.*, *299*, 242–249, doi:10.1016/j.epsl.2010.09.004, 2010.